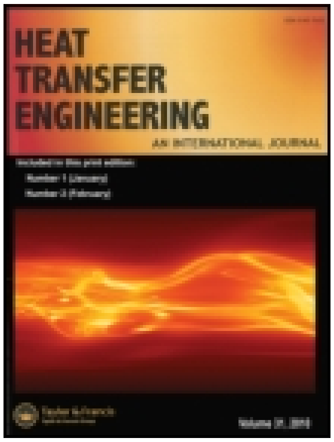

Heat Transfer Engineering
Publication details, including instructions for authors and subscription information:
http://www.tandfonline.com/loi/uhte20

Numerical Simulation of Transpiration Cooling for Sintered Metal Porous Strut of the Scramjet Combustion Chamber

Yan-Bin Xiong [a] , Yin-Hai Zhu [a] & Pei-Xue Jiang [a]
[a] Key Laboratory for Thermal Science and Power Engineering of Ministry of Education, Department of Thermal Engineering , Tsinghua University , Beijing , China
Accepted author version posted online: 02 Sep 2013.Published online: 25 Nov 2013.

To cite this article: Yan-Bin Xiong , Yin-Hai Zhu & Pei-Xue Jiang (2014) Numerical Simulation of Transpiration Cooling for Sintered Metal Porous Strut of the Scramjet Combustion Chamber, Heat Transfer Engineering, 35:6-8, 721-729, DOI: 10.1080/01457632.2013.837790

To link to this article: http://dx.doi.org/10.1080/01457632.2013.837790

Heat Transfer Engineering, 35(6–8):721–729, 2014

ISSN: 0145-7632 print / 1521-0537 online
DOI: 10.1080/01457632.2013.837790

Taylor & Francis
Taylor & Francis Group

Numerical Simulation of Transpiration Cooling for Sintered Metal Porous Strut of the Scramjet Combustion Chamber

YAN-BIN XIONG, YIN-HAI ZHU, and PEI-XUE JIANG
Key Laboratory for Thermal Science and Power Engineering of Ministry of Education, Department of Thermal Engineering, Tsinghua University, Beijing, China

The strut structure in a scramjet combustion chamber is used to inject fuel into the main stream. The environment surrounding the strut in the scramjet chamber is supersonic flow at very high temperatures. Thus, the leading edge of the strut is easily ablated due to aerodynamic heating. This study analyzes the effect of a transpiration cooling scheme using a sintered metal porous media surface to protect the strut from ablation. Numerical simulations are used to study the transpiration cooling for different strut structures and coolant conditions. The influences of these parameters on the transpiration cooling of the strut are analyzed for a main stream Mach number of 2.5 and a total temperature of 1700 K. The surface temperature can be reduced to a safe temperature with a coolant mass flow rate through the porous media of 27.5 kg/ m^2-s. The coolant flow near the leading edge is most important, with less flow needed downstream.

INTRODUCTION

The scramjet is one of the most promising propulsion systems for hypersonic transport in next-generation high-speed transports. Since the detention time of the oxidizer stream in the combustion chamber is several milliseconds, an effective injection scheme must be designed to provide rapid mixing. In some scramjet engines, struts have been installed in the combustion zone to inject the fuel into the main stream to improve mixing. Many studies have focused on the effects of the mixing and the aerodynamic performance with the strut. Tani et al. [1] experimentally studied the aerodynamic influence of the strut between the side walls. Their experimental results showed that the additional shock waves generated by the strut created a large separation zone on the side walls, which reduced the total pressure efficiency and the capture ratio. Boyce et al. [2] compared supersonic combustion experiments in a vitiation-heated blow-down tunnel in Japan and a free-piston shock tunnel in Australia with a strut in the combustion chamber. Their results showed that the difference between the two facilities is within the experimental error when the different freestream and boundary-layer effects are included. Masuya et al. [3] experimentally investigated the ignition and combustion performance of a scramjet combustor with a fuel injection strut to show that the plasma igniters could successfully ignite both parallel and perpendicular fuel jets without a noticeable time delay between the two sides of the strut. Other studies have considered fuel mixing and the effects of the strut on the combustion [4–6].

The environment around the strut in the scramjet chamber has supersonic flow at very high temperatures. Thus, the leading edge of the strut suffers severe ablation due to aerodynamic heating. There have been several studies of thermal protection methods for the strut, especially for the leading edge. Motoyama et al. [7] suggested a spike attached to a hemispherical body to change the flow structure to reduce the heat flux and pressure drag by generating a recirculation region around the stagnation point. Bouchez et al. [8] described the activities of the French PATH-SOCAR work using fuel-cooled composite material structures in dual-mode ramjets for thermal protection. They gave experimental and numerical results for the thermal protection for scramjet applications using C/SiC materials.

This project was supported by the National Natural Science Foundation of China (No. 51276094), the Science Fund for Creative Research Groups (No. 51321002) and the Defense Industrial Technology Development Program (No. B1420110113).

Address correspondence to Professor Pei-Xue Jiang, Department of Thermal Engineering, Tsinghua University, Beijing, 100084, China. E-mail: jiangpx@tsinghua.edu.cn

Sun and Zheng [9] numerically studied the thermal protection effectiveness of three thermal protection schemes using a regeneration cooling scheme, a C/SiC thermal protection material, and gas jet thermal protection. Their results showed that for high Mach numbers, regeneration cooling and C/SiC thermal protection cannot protect the leading edge so gas jet cooling must be used.

Transpiration cooling is one of the most efficient cooling techniques to protect surfaces from very hot gas streams and is well recognized as a possible means for cooling rocket combustion walls, gas turbine combustion chambers and blades. Thus, transpiration cooling is also a plausible solution for thermal protection of the strut. There have been several studies of transpiration cooling for scramjet engines [10–12].

This paper describes a transpiration cooling scheme using a sintered metal porous medium to protect the strut from ablation. Numerical simulations are used to study the transpiration cooling for different strut structures and coolant conditions.

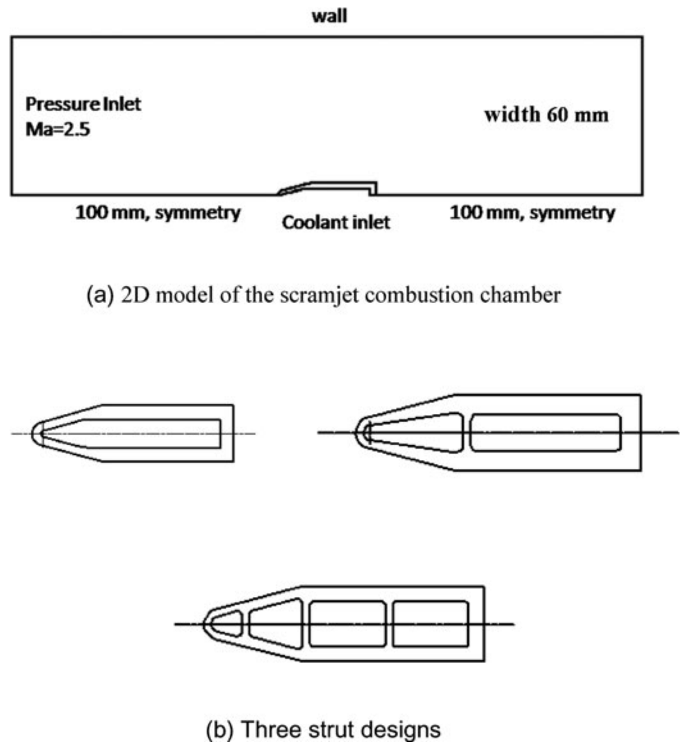

Figure 1 Model of the struts in the scramjet combustion chamber.

PHYSICAL MODEL

In some previous experimental studies, the strut height was the same as the scramjet channel height with the strut passing completely through the channel [2, 13]. In addition, the strut height is usually much larger than the strut thickness. The model has been simplified to reduce the computations by using a two-dimensional (2D) model or periodic boundary conditions using a portion of the model with the vertical direction in a three-dimensional model [14, 15]. Figure 1a shows the 2D model of the scramjet combustion chamber used in the present calculations with a strut made of sintered stainless-steel particles installed in the center of the domain. Simulations comparing the symmetric 2D model with an entire 2D model showed little difference between the surface temperatures and flow fields predicted by the two models. Therefore, the symmetry boundary condition was used for the simulations. The flow inlet was 60 mm wide and the computational domain extended 100 mm in front of and behind the strut. The three strut geometries employed in the simulation are shown in Figure 1b. The external contours are the same for the three structures with a 10-mm-thick strut with a 30-degree blunt wedge on the upstream side to deflect the oncoming flow. The struts were 37.5 mm long. The leading edge had a 2-mm radius and was 1 mm thick with a body wall thickness of 2.5 mm for structures 1 and 2 and 2 mm for structure 3. The internal structures had one rib to strengthen the strut in the strut cavity in model 2 and three ribs in model 3. The leading edge of the strut always had the highest temperature on the strut surface, with the surface temperature decreasing to a relatively low value along the flow direction. One way to reduce the leading edge temperature is to increase the cavity pressure next to the leading cone to increase the leading edge mass flow rate, which will reduce the temperature. The incoming hot supersonic stream was set to be air, with methane fuel used for the coolant. Thus, after the transpiration cooling of the strut, the methane mixes with the main stream and combusts.

The main stream and coolant fuel inlet boundary conditions were set to those given by Dessornes and Jourden [16], with mainstream inlet conditions of Ma = 2.5, P_0 = 1.0 MPa, and T_0 = 1700 K. These were kept constant for all the simulation structures. The walls were assumed to be insulated with a no-slip boundary condition. The outlet of the computational domain was specified as a pressure outlet. The air and methane were treated as ideal gases, with polynomials used for their thermal conductivities, specific heats, and viscosities. The species mixing model was based on kinetic theory [17]. The porous material was assumed to be stainless steel.

The mass flux boundary condition was used for the internal coolant inlets, with three mass fluxes, 27.5 kg/m^2-s, 55 kg/m^2-s, and 68.75 kg/m^2-s used at each inlet boundary to achieve mass flow rates of about 1 kg/s, 2 kg/s, and 2.5 kg/s. These three mass fluxes are referred to as fluxes I, II, and III in the following.

MATHEMATICAL MODEL AND NUMERICAL METHOD

The simulations used the commercial software FLUENT version 12, which uses the Favre-averaged equations to solve the continuity, momentum, energy, and mass transport equations for supersonic flow. The Spalart–Allmaras (SA) turbulent model, which was designed specifically for aeronautics and aerospace applications involving wall-bounded flows and has been shown to give fairly good agreement for various supersonic and hypersonic flow patterns, was used for the turbulent closure. Bardina et al. [18] compared the performance of the k-ω model of Wilcox, the k-ε model of Launder and Sharma, the k-ω SST model of Menter, and the S-A model of Spalart and Allmaras to show that for five free shear flows and five boundary-layer flows, the Spalart-Allmaras and SST model gave the best numerical predictions. For the 2D mixing layers, wake flows, and flat-plate boundary-layer simulations, the SA model gave better predictions. For this study, the boundary-layer development on the strut surface and the flow structure in the wake are most important, so the SA model was used for the turbulence. Large-eddy simulation (LES) results by Génin and Menon [14] showed that the flow field is unsteady in the wake of the bluff body with vortical structures that contribute to the mixing of the hydrogen jet with the recirculating fluid. In addition, their simulation results also indicated that the time-averaged flow features showed reasonable agreement with experimental results. The shock pattern was found to be rather steady and insensitive to the dynamics of the recirculating region and of the shear layers. In this study, the shock pattern should be steady for the constant main stream inlet and coolant inlet conditions. The unsteady vortices formed in the strut wake should have little effect on the surface temperatures, especially in front of the strut. Thus, the cases in this study were calculated assuming steady-state conditions.

The governing equations for this 2D, steady, and compressible problem are:

Continuity equation:

$$\frac{\partial}{\partial x}(\rho u) + \frac{\partial}{\partial y}(\rho v) = 0 \tag{1}$$

Momentum equation in the x direction:

$$\begin{aligned}\frac{\partial}{\partial x}(\rho uu) + \frac{\partial}{\partial y}(\rho vu) &= \frac{\partial}{\partial x}\left[(\eta+\eta_t)\frac{\partial u}{\partial x}\right] + \frac{\partial}{\partial y}\left[(\eta+\eta_t)\frac{\partial u}{\partial y}\right] - \frac{\partial p}{\partial x} \\ &+ \frac{\partial}{\partial x}\left[(\eta+\eta_t)\frac{\partial u}{\partial x}\right] + \frac{\partial}{\partial y}\left[(\eta+\eta_t)\frac{\partial v}{\partial x}\right]\end{aligned} \tag{2}$$

Momentum equation in the y direction:

$$\begin{aligned}\frac{\partial}{\partial x}(\rho uv) + \frac{\partial}{\partial y}(\rho vv) &= \frac{\partial}{\partial x}\left[(\eta+\eta_t)\frac{\partial v}{\partial x}\right] + \frac{\partial}{\partial y}\left[(\eta+\eta_t)\frac{\partial v}{\partial y}\right] - \frac{\partial p}{\partial x} \\ &+ \frac{\partial}{\partial x}\left[(\eta+\eta_t)\frac{\partial u}{\partial y}\right] + \frac{\partial}{\partial y}\left[(\eta+\eta_t)\frac{\partial v}{\partial y}\right]\end{aligned} \tag{3}$$

Energy equation:

$$\begin{aligned}\frac{\partial}{\partial x}(\rho uT) + \frac{\partial}{\partial y}(\rho vT) &= \frac{\partial}{\partial x}\left[\left(\frac{\eta}{\Pr} + \frac{\eta_t}{\sigma_t}\right)\frac{\partial T}{\partial x}\right] \\ &+ \frac{\partial}{\partial y}\left[\left(\frac{\eta}{\Pr} + \frac{\eta_t}{\sigma_t}\right)\frac{\partial T}{\partial y}\right]\end{aligned} \tag{4}$$

The SA turbulent model defines the turbulent viscosity function in terms of an eddy viscosity, $\tilde{\nu}$, and a wall function, $f_{\nu l}$, as:

$$\eta_t = \rho\tilde{\nu} f_{vl} \tag{5}$$

The convective transport equation for the eddy viscosity is:

$$\begin{aligned}\frac{\partial \rho\tilde{\nu}}{\partial t} + \frac{\partial(\rho\tilde{\nu}u_j)}{\partial x_j} &= c_{b1}(1-f_{t2})\rho\tilde{S}\tilde{\nu} \\ &+ \frac{1}{\sigma}\left[\frac{\partial}{\partial x_j}\left(\rho(\nu+\tilde{\nu})\frac{\partial\tilde{\nu}}{\partial x_j}\right) + c_{b2}\rho\frac{\partial\tilde{\nu}}{\partial x_j}\frac{\partial\tilde{\nu}}{\partial x_j}\right] \\ &- \left[c_{w1}f_w - \frac{c_{b1}}{\kappa^2}f_{t2}\right]\rho\left(\frac{\tilde{\nu}}{d}\right)^2 + f_{t1}\rho\Delta U^2\end{aligned} \tag{6}$$

Here S is the magnitude of the vorticity and d is the distance to the closest wall. The subscript b stands for "basic," w stands for "wall," v stands for "viscous," and t stands for "trip," which means the start of transition. Detailed definitions for the model can be found in Spalart and Allmaras [19].

The Brinkman–Forchheimer extended Darcy equation was used to model the coolant flow through the porous media as

$$\nabla(\rho_f \varepsilon u) = -\nabla P + \nabla(\rho_f \mu u) - \frac{\mu_f}{K}\varepsilon^2 u - \varepsilon^3\frac{\rho_f F}{\sqrt{K}}|u|u \tag{7}$$

The permeability, K, and the inertia coefficient, F, were given by Ergun [20]:

$$K = \frac{d_p^2\cdot\varepsilon^3}{150(1-\varepsilon)^2},\; F = \frac{1.75}{\sqrt{150}\varepsilon^{3/2}} \tag{8}$$

The solid and fluid temperatures in the porous media are not actually the same, with many analyses of the solid and fluid temperature distributions in porous media using various simplifications and boundary conditions for transpiration cooling [21–24]. Wang and Wang [21] gave a conservative quantitative criterion for use of the LTE model as

$$M < 0.223Bi^{0.507} \tag{9}$$

where M is the dimensionless coolant mass flow rate, $M = mc_{pf}H/k_{se}$, and Bi is the pore Biot number, $Bi = h_{sf}a_{sf}H^2/k_{se}$. The criterion is satisfied for all the cases considered here; thus, thermal equilibrium model was used in this study. The thermal equilibrium model has been proven to be an effective method

Table 1 Calculated temperatures for the three meshes

	Coarse mesh	Fine mesh	Finer mesh
Cells before adaption	94382	152647	220189
Cells after adaption	112452	173846	237543
Leading edge temperature	1259.6	1256.8	1256.1

Table 2 Comparison theoretical and numerical values of Δ and T_0

	Stand-off distance Δ, mm	Stagnation temperature T_0, K
Theoretical	1.630	1700
Numerical	1.657	1703.3
Difference	1.66%	0.19%

for transpiration cooling numerical simulation research when coupled with the mainstream flows [25, 26]. The energy equation in the porous media for this model is

$$\nabla(\rho_f c_{pf} \varepsilon u T_f) = \nabla((\lambda_m + \lambda_d)\nabla T_f) \tag{10}$$

The effective thermal conductivity for the porous media, λ_m, with consideration of the thermal dispersion is defined as [27]

$$\frac{\lambda_m}{\lambda_f} = (1 - \sqrt{1-\varepsilon}) + \frac{2\sqrt{1-\varepsilon}}{1-\sigma B} \times \left[\frac{(1-\sigma)B}{(1-\sigma B)^2}\ln\left(\frac{1}{\sigma B}\right) - \frac{B+1}{2} - \frac{B-1}{1-\sigma B}\right] \tag{11}$$

$$B = 1.25\left(\frac{1-\varepsilon}{\varepsilon}\right)^{\frac{10}{9}}, \sigma = \frac{\lambda_f}{\lambda_s} \tag{12}$$

The additional thermal conductivity, λ_d, due to the thermal dispersion in porous media was [28]

$$\lambda_d = C\rho_f c_{pf} d_p U_p (1-\varepsilon), C = 1.60[\mathrm{Re}_p \cdot \mathrm{Pr}_f \cdot (1-\varepsilon)]^{0.8282} \tag{13}$$

The mesh adaption function in FLUENT was used to refine the mesh around the shock wave to more accurately catch the shock wave. Three meshes for strut structure 2 were formed to get a fine mesh that balanced the accuracy and computational load. The surface temperatures with coolant mass flux I indicated that the largest temperature difference occurred at the leading edge of the strut, with the difference getting smaller along the surface. The leading edge temperature for the different meshes is shown in Table 1. The grid near the strut after adaption for the fine mesh is shown in Figure 2.

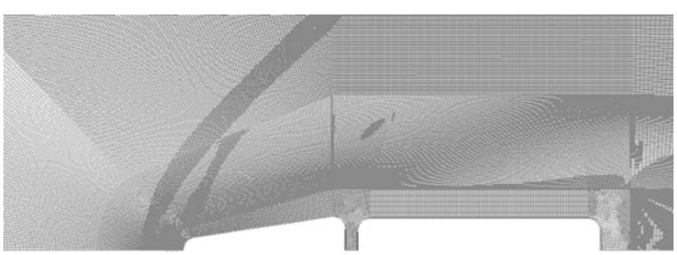

Figure 2 Typical of the Mach number contours.

RESULTS AND DISCUSSION

Two key parameters, Δ and T_0, from numerical results without transpiration cooling were compared with predictions of theoretical and empirical equations to check the accuracy of the simulations. Δ denotes the detached shock stand-off distance in front of the body, while T_0 is the stagnation temperature at the leading edge of the strut. Ambrosio and Wortman [29] correlated experimental results for the stand-off distance for the wedge-cylinders as

$$\Delta/R = 0.386\exp(4.67/M^2) \tag{14}$$

where Δ is the stand-off distance, R is the radius of the wedge-cylinder, and M is the Mach number. The air temperature of the first element near the stagnation point was used for the stagnation temperature. The results in Table 2 show that the numerical results correspond well with the theoretical values.

The numerical Mach number contours for the three structures are shown in Figure 3. The Mach 2.5 incoming flow is deflected at the tip of the strut to form an oblique shock wave. After impacting the upper walls, the oblique shocks reflect back downstream toward the chamber centerline.

Figure 4 compares the Mach number contours around the struts with and without transpiration cooling for the three structures. The Mach number contours are very concentrated near the strut surface without transpiration cooling, which means there are very large velocity gradients. The transpiration from the surface significantly reduces the velocity gradients for all these structures.

The temperature contours for the three structures in Figure 5 show that the strut surface temperatures are lower than the oncoming stream temperature. The leading edge temperature at the strut surface without transpiration reached the total temperature of the oncoming stream. The air kinetic energy is

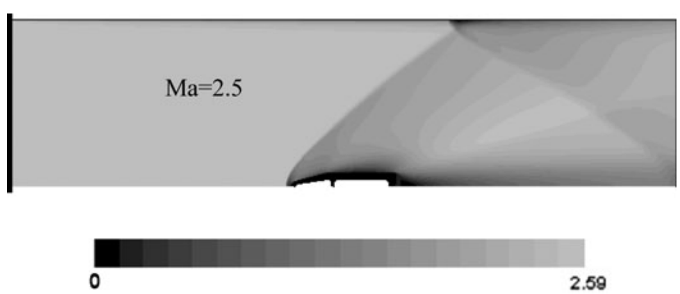

Figure 3 Mach number contours, with (upper half) and without transpiration (lower half).

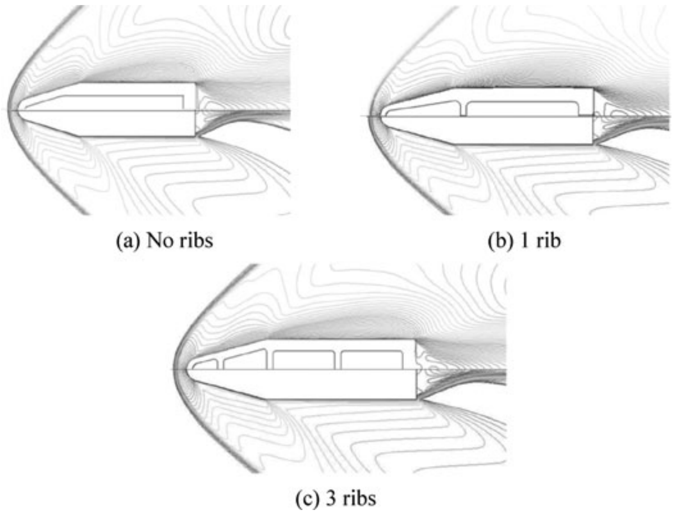

Figure 4 Contours of temperature with (upper half) and without transpiration (lower half).

transformed to molecular thermal motion energy due to the viscous flow and strong shock compression, which makes the strut leading edge surface temperature the highest in the whole computational domain. However, the strut surface temperature with transpiration was much lower with the velocity stagnation point moved ahead of the leading edge of the struts, as the transpiration coolant pushed the stagnation point away from the surface. The strong compression shock ahead of the leading edge of the strut caused the highest temperature to occur just in front of the strut leading edge. Downstream, the surface gas velocity was not zero due to continued injection, which reduced the aerodynamic heating.

Figure 6 shows the methane mass fraction contours around the struts. The contours show that as more coolant flowed from the porous strut surface, the methane layer became thicker as it moved downstream along the surface, which effectively reduced the heat transfer. Thus, the continuous methane injection from the porous wall thickens the boundary layer and isolates the surface from the hot stream.

The different coolant blowing ratios had some effects on the contours. As can be seen in Figure 7, the boundary-layer thickness increases with increasing coolant mass flow rate. The thicker boundary layers push the stagnation point further from the leading edge and accumulate more methane coolant along the downstream surface. Thus, the temperatures along the strut surface decrease as the blowing ratio increases.

Figure 8 shows the strut surface temperatures along the surface for different mass flow rates and the different structures. The temperature trends are similar to those in Figure 5 for the three structures. The temperature is highest at the leading edge

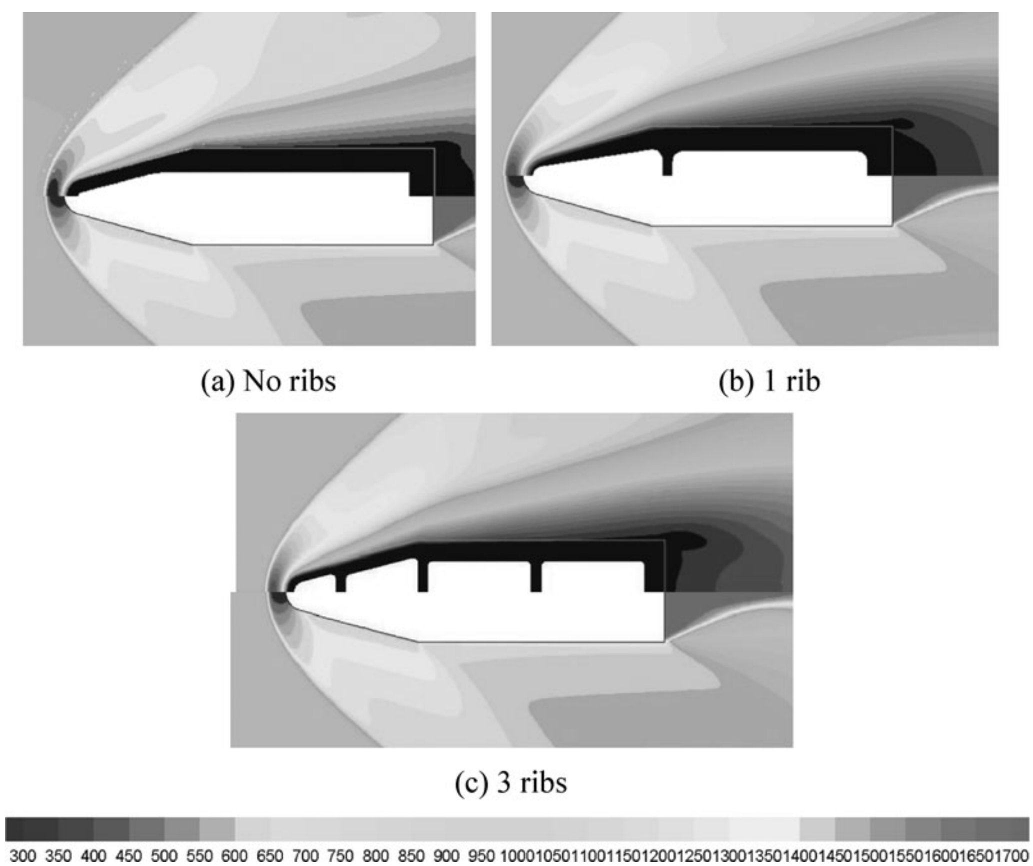

Figure 5 Methane mass fraction contours.

(a) No ribs

(b) 1 rib

(c) 3 ribs

Figure 6 Methane mass fraction contours for different mass fluxes for structure 2.

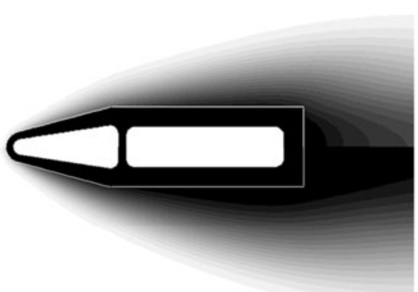

(a) Mass flux Ⅰ (upper) vs Ⅱ (lower)

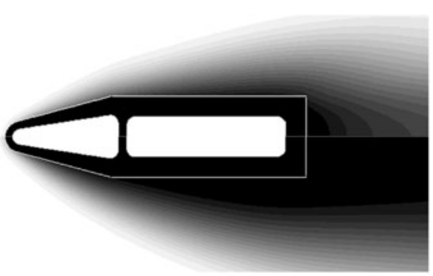

(b) Mass flux Ⅰ (upper) vs Ⅲ (lower)

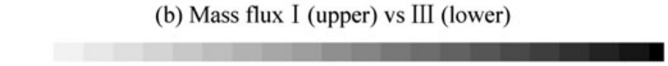

Figure 7 Temperature variations along the strut surface.

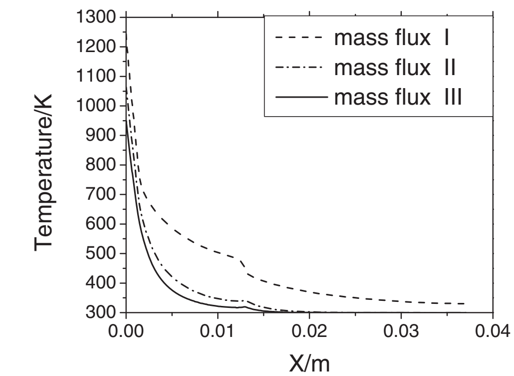

Structure 1

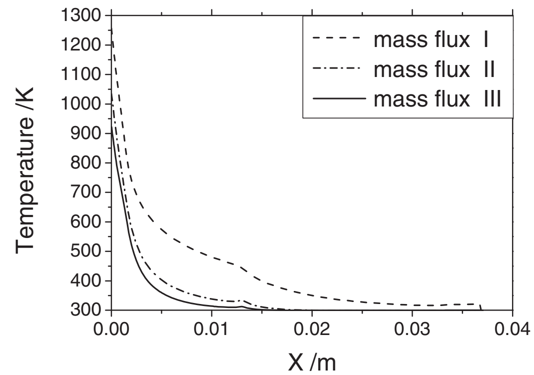

Structure 2

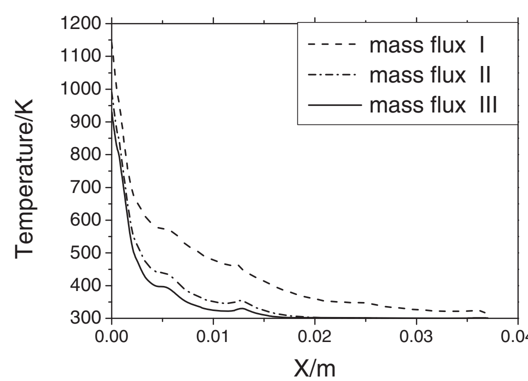

Structure 3

Figure 8 Temperature variations for variables mass fluxes.

of the strut and decreases sharply along the surface. For structures 2 and 3, the downstream surface temperature drops to the coolant inlet temperature, 300 K, which is not necessary; thus, some coolant is wasted. The highest temperature for these three structures is 1257 K for structure 2 for mass flux I, which is acceptable for the material so the higher mass fluxes are not needed.

Increasing the coolant inlet mass flux reduces the leading edge temperature, which is the most critical point for the strut. However, Figure 8 shows that for a large mass flux, the

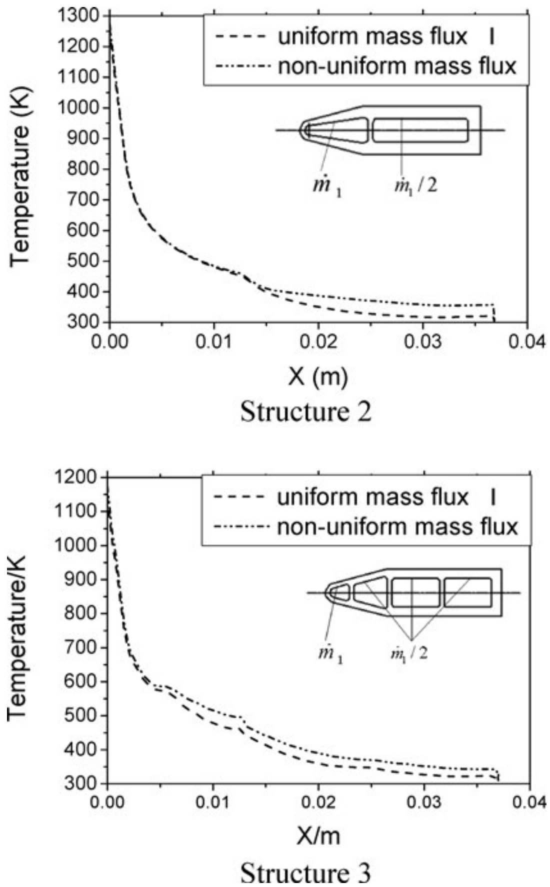

Figure 9 Cooling effectiveness along the strut.

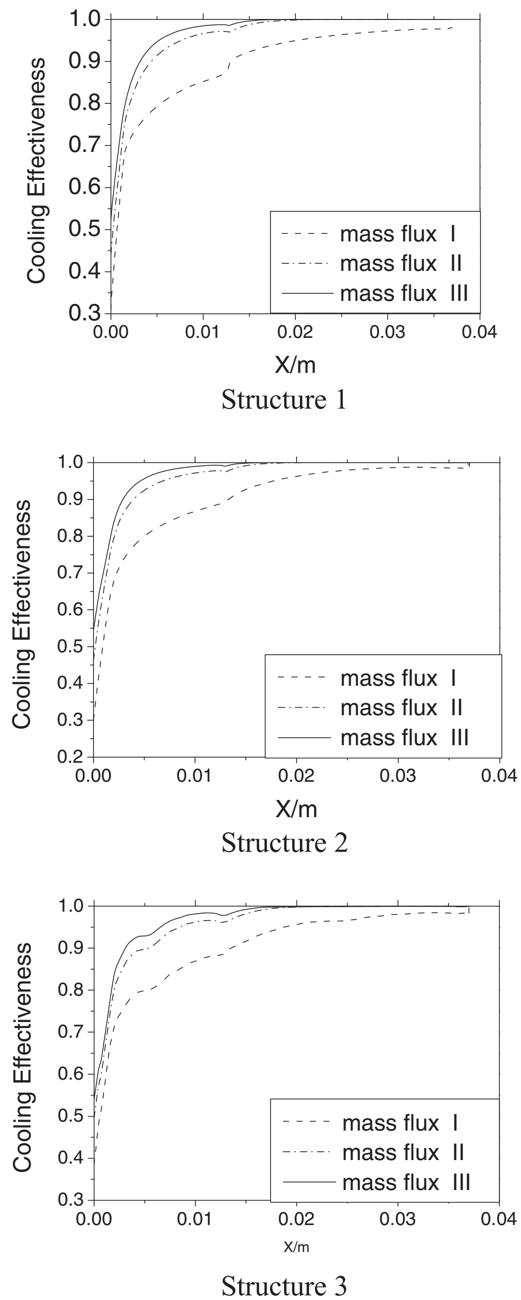

Figure 10 Cooling effectiveness variations with variable mass fluxes.

temperature decreases little with increasing coolant mass flux, which means the increased flow rate is not necessary. Figure 9 shows the temperature variation for a nonuniform mass flux for the different internal cavities. For structure 2, the fore cavity mass flux was kept at 27.5 kg/m^2-s, while the aft cavity mass flux was reduced by half. For structure 3, the fore cavity mass flux was also kept at 27.5 kg/m^2-s, while the mass fluxes in the other three cavities were reduced by half. For both structures, decreasing the aft cavity inlet coolant mass fluxes resulted in temperature increases on the afterbody outer surfaces, with little variation of the front surface temperatures. The temperature increases were very small and acceptable for the material, which means that the nonuniform mass fluxes can provide effective protection with less coolant. The permeability of the leading edge could be increased or a hole could be drilled in the leading edge to further reduce the surface temperatures.

In supersonic transpiration cooling, the cooling effectiveness, η, is defined as

$$\eta = \frac{T_r - T_w}{T_r - T_c} \tag{15}$$

where T_c is the coolant temperature and T_r is the free stream recovery temperature, defined as

$$T_r = T_\infty \left(1 + r\frac{\gamma - 1}{2} Ma^2\right) \tag{16}$$

where r is the recovery factor and γ is the specific heat ratio.

The cooling effectiveness along the surface is plotted in Figure 10. The cooling effectiveness around the leading edge is very poor and should be improved.

The cooling effectiveness variations for the nonuniform mass flux cases are shown in Figure 11. These results also show that increasing the local mass flux at the leading edge provides effective protection with less coolant usage.

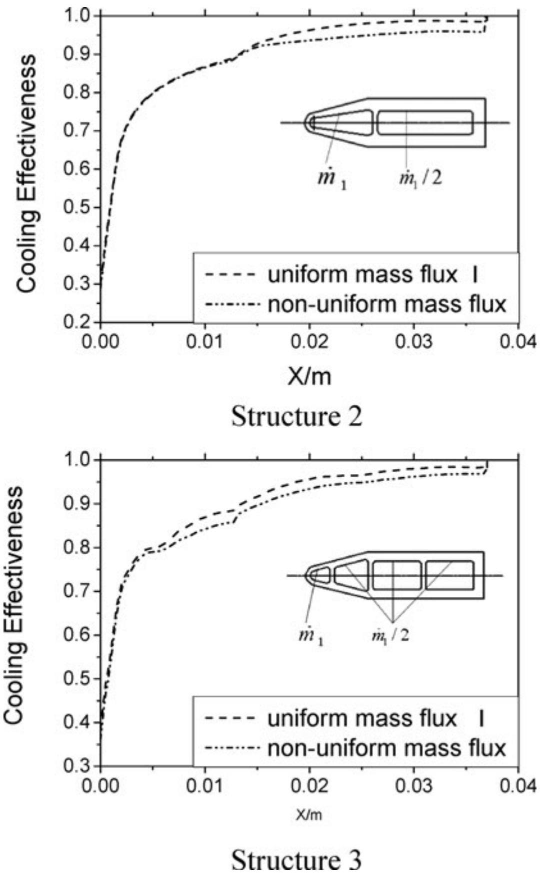

Figure 11 Cooling effectiveness variations with variable mass fluxes.

CONCLUSIONS

Numerical simulations were used to study the transpiration cooling of struts in scramjets made of a sintered metal porous media. The conclusions are:

1. The thermal environment around the strut in the scramjet combustion chamber is very severe. Active cooling must be used to protect the strut to provide a long lifetime.
2. Injection from the leading edge into the flow stream pushes the stagnation point away from the surface. A thin film of low-temperature coolant is established at the leading edge, which provides effective thermal protection from the oncoming hot stream. Near the downstream strut surface, the air velocity is not zero due to the flow injection, which reduces the aerodynamic heating.
3. A higher local mass flux at the leading edge with less transpiration cooling downstream provides effective protection with less coolant flow.
4. Additional cooling will be needed to protect the strut leading edge as the mainstream temperatures become higher.

NOMENCLATURE

d_p particle diameter [m]
F inertia coefficient
f_{vl} wall function for the SA model
K permeability of the porous media [Darcy]
$\dot{m}$ mass flux
Ma Mach number
P_0 total pressure [Pa]
Pr Prandtl number
T, T_0 temperature, total temperature [K]
u, v velocity in the x or y directions [m/s]
U_p absolute pore velocity ($Up = (u_p^2 + v_p^2)^{1/2}$) [m/s]
x, y, z coordinate directions [m]

Greek Symbols

λ thermal conductivity [W/(m-K)]
μ dynamic viscosity [N-s/m^2]
η cooling effectiveness
η_t turbulent viscosity, [N-s/m^2]
$\tilde{\upsilon}$ eddy viscosity in the SA model
ε porous media porosity
γ specific heat ratio
ρ density [kg/m^3]

Subscripts

f fluid
p particle
r recovery factor

REFERENCES

[1] Tani, K., Kanda, T., and Tokunaga, T., Aerodynamic Performance of Scramjet Inlet Models With a Single Strut, *Journal of Propulsion and Power*, vol. 22, no. 3, pp. 905–912, 2006.
[2] Boyce, R. R., Paull, A., Stalker, R. J., Wendt, M., Chinzei, N., and Miyajima, H., Comparison of Supersonic Combustion Between Impulse and Vitiation-Heated Facilities, *Journal of Propulsion and Power*, vol. 16, no. 4, pp. 709–717, 2000.
[3] Masuya, G., Komuro, T., Murakami, A., Shinozaki, N., Nakumura, A., Murayama, M., and Ohwaki, K., Ignition and Combustion Performance of Scramjet Combustors With Fuel Injection Struts, *Journal of Propulsion and Power*, vol. 11, no. 2, pp. 301–307, 1995.
[4] Sullins, G., Anderson, J., and Drummond, J., Numerical Investigation of Supersonic Base Flow With Parallel Injection, *AIAA paper 82–1001*, June 1982.
[5] Pandey, K. M., and Sivasakthivel, T., CFD Analysis of Mixing and Combustion of a Scramjet Combustor With a Planer Strut Injector, *International Journal of Environmental Science and Development*, vol. 2, no. 2, pp. 102–108, 2011.

[6] Bayley, D., and Hartfield, R., Experimental Investigation of Angled Injection in a Compressible Flow, *AIAA paper 95–2414*, July 1995.

[7] Motoyama, N., Mihara, K., Miyajima, R., Watanuki, T., and Kubota, H., Thermal Protection and Drag Reduction With Use of Spike in Hypersonic Flow, *AIAA paper 2001–1828*, April 2001.

[8] Bouchez, M., Cahuzac, G., and Beyer, S., PTAH-SOCAR Fuel-Cooled Composite Materials Structure in 2003. *AIAA-2003–6919*, August 2003.

[9] Sun, B., and Zheng, L.M., Research of Scramjet Strut Thermal Environment and Thermal Protection Scheme, *Journal of Aerospace Power*, vol. 21, no. 2, pp. 336–341, 2006.

[10] Kulkarni, P. S., Ravi, B. R., and Reddy, K. P. J., Two Dimensional Navier–Stokes Solutions for Transpiration Cooling at Hypersonic Mach Numbers, *Shock Waves*, vol. 13, pp. 497–500, 2004.

[11] Sreekanth, and Reddy, N. M., Numerical Simulation of transpiration Cooling Over Blunt Bodies at Hypersonic Mach Numbers, *30th AIAA Thermophysics Conference June 19–22, AIAA 95–2082*, San Diego, CA, 1995.

[12] Foreest, A. V., Sippel, M., Klevanski, J., Gülhan, A., and Esser, B., Transpiration Cooling to Handle the Aerothermodynamic Challenges of the Spaceliner Concept, *2nd European Conference For Aerospace Sciences (Eucass)*, 2007.

[13] Tomioka, S., Kandaf, T., Tani, K., Mitani, T., Shimuraf, T., and Chinzei, N., Testing of a Scramjet Engine With a Strut at M8 Flight Condition, *AIAA paper 98–3134*, 1998.

[14] Genin, F., and Menon, S., Simulation of Turbulent Mixing Behind a Strut Injector in Supersonic Flow, *AIAA Journal*, vol. 48, no. 3, pp. 526–539, 2010.

[15] Oevermann, M., Numerical Investigation of Turbulent Hydrogen Combustion in a SCRAMJET Using flamelet Modeling, *Aerospace Science and Technology*, vol. 4, no. 7, pp. 463–480, 2000.

[16] Dessornes, O., and Jourdren, C., Mixing Enhancement Techniques in a Scramjet, *AIAA Paper 1998–1517*, ONERA, 1998.

[17] Hirschfelder, J. O., Curtiss, C. F., and Bird, R. B., *The Molecular Theory of Gases and Liquids*, Wiley, New York, NY, 1964.

[18] Bardina, J. E., Huang, P. G., and Coakley, T. J., Turbulence Modeling Validation, Testing, and Development, *NASA Technical Memorandum* 110446, April 1997.

[19] Spalart, P. R., and Allmaras, S. R., A One Equation Turbulence Model for Aerodynamic Flows, *AIAA paper 92–0439*, 1992.

[20] Ergun, S., Fluid Flow Through Packed Columns, *Chemical Engineering Progress*, vol. 48, no. 2, pp. 89–94, 1952.

[21] Wang, J. H., and Wang, H. N., A Discussion of Transpiration Cooling Problems Through an Analytical Solution of Local Thermal Nonequilibrium Model, *Journal of Heat Transfer*, vol. 128, no. 10, pp. 1093–1098, 2006.

[22] Colladay, R. S., and Stepka, F. S., Examination of Boundary Conditions for Heat Transfer Through a Porous Wall, *NASA Technical Note D-6405*, 1971.

[23] Weinbaum, S., and Wheeler, H. L., Heat Transfer in Sweat-Cooled Porous Metals, *Journal of Applied Physics*, vol. 20, issue 1, 1949.

[24] Wolfersdorf, J. V., Effect of Coolant Side Heat Transfer on Transpiration Cooling, *Heat and Mass Transfer*, vol. 41, no. 4, pp. 327–337, 2005.

[25] Jia, S., *An Investigation of Transpiration Cooling Performance in Curved Boundary Layer*, Master's thesis, University of Science and Technology of China, Beijing, China, 2009.

[26] Liu, Y. Q., Jiang, P. X., Jin, S. S., and Sun, J. G., Transpiration Cooling of a Nose Cone By Various Foreign Gases, *International Journal of Heat and Mass Transfer*, vol. 53, no. 23–24, pp.5364–5372, 2010.

[27] Hunt, M. L., and Tien, C. L., Non-Darcy Convection in Cylindrical Packed Beds, *Journal of Heat Transfer*, vol. 110, pp. 378–384, 1988.

[28] Jiang, P. X., Ren, Z. P., and Wang, B. X., Numerical Simulation of Forced Convection Heat Transfer in Porous Plate Channels Using Thermal Equilibrium and Nonthermal Equilibrium Models, *Numerical Heat Transfer, Part A, Applications*, vol. 35, no. 1, pp. 99–113, 1999.

[29] Ambrosio, A., and Wortman, A., Stagnation Point Shock Detachment Distance for Flow Around Spheres and Cylinders, *ARS Journal*, vol. 32, p. 281, 1962.

Yan-Bin Xiong is a Ph.D. student in the Department of Thermal Engineering, Tsinghua University, China. He received his B.E. from Huazhong University of Science and Technology in 2008. His main research interests are transpiration cooling and film cooling.

Yin-Hai Zhu is an assistant professor in the Department of Thermal Engineering, Tsinghua University, China. He received his Ph.D. in engineering thermophysics from Xi'an Jiaotong University in 2009. His main research interests are refrigeration and cryogenics systems and spacecraft thermal protection.

Pei-Xue Jiang is a professor in the Department of Thermal Engineering, Tsinghua University, China.. He received his Ph.D. in the Department of Thermo-Power Engineering of Moscow Power Engineering Institute in 1991. He then joined the faculty of Tsinghua University and took the professor post in 1997. His main research interests include convection heat transfer in porous media and enhanced heat transfer, convection heat transfer at supercritical pressures, transpiration cooling and film cooling, thermal transport in nanoscale structures, trans-critical CO_2 air conditioning systems, and heat pumps. He has published more than 100 papers in international journals and conferences.